Journal of Luminescence 226 (2020) 117425

Contents lists available at ScienceDirect

Journal of Luminescence

journal homepage: http://www.elsevier.com/locate/jlumin

Sequential two-step optical stimulation in K-feldspars: Correlation among the luminescence signals and implications for modeling parameters

Vasiliki Angeli [a,*], George Kitis [a], Vasilis Pagonis [b], Georgios S. Polymeris [c,d]

[a] Aristotle University of Thessaloniki, Nuclear Physics Laboratory, 54124, Thessaloniki, Greece
[b] McDaniel College, Physics Department, Westminster, MD, 21157, USA
[c] Institute of Nuclear Sciences, Ankara University, Beşevler, 06100, Ankara, Turkey
[d] Institute of Nanoscience and Nanotechnology, NCSR "Demokritos", Ag. Paraskevi, 15310, Athens, Greece

ARTICLE INFO

Keywords:
Feldspars
BLOSL/IRSL
Tunneling recombination
Crystal structure
Dimensionless density parameter
Unit cell volume

ABSTRACT

Luminescence signals from feldspars are of importance in luminescence dosimetry and dating. The present study attempts a correlation between two specific experimental parameters, such as the lifetime of luminescence components and the dimensionless acceptor density parameter ρ', as well as the influence of the crystal structure on the luminescence signals. The analysis of the above parameters was completed in three different K-feldspar samples, each one belonging to the structural group of microcline, sanidine and orthoclase. The stimulations in this manuscript were carried out using blue optically stimulated luminescence (BLOSL) and infrared (IRSL) optically stimulated luminescence, in two different two step experimental protocols. A comparison of these two step protocols is applied for the first time in the literature. A de-convolution analysis was completed with the use of two components, a slow component which can be described by general order kinetics (GOK), and a tunneling component which is necessary to describe the blue light stimulation. The GOK component describes recombination processes taking place only through the conduction band. In order to describe the results of the IR stimulation protocol, two tunneling components were used. The results from this study are encouraging and are in full correlation with published studies in the luminescence literature.

1. Introduction

Thermoluminescence (TL) glow curves, as well as blue optically stimulated luminescence (BLOSL) and infrared optically stimulated luminescence (IRSL) decay curves from feldspars and quartz, have been studied extensively in retrospective dosimetry applications, including archeological and geological dating and accidental dosimetry. Feldspars and quartz are the most widespread minerals in the crust of Earth, as well as the most established naturally occurring luminescence phosphors, due to their very good dosimetric properties. The feldspar mineral has a wide band-gap of around 7.7 eV [1] and contains many defects that can store charge over geological time scales. The TL and IRSL signals from feldspars have been extensively studied because of their excellent repeatability and sensitivity, and also because they can be found in various rock types, of igneous, sedimentary and metamorphic origin [2–4].

It has now been established that two different types of transitions can take place in these minerals; delocalized transitions occurring via the conduction and valence bands, and also localized transitions [5]. In localized transitions, electrons are optically or thermally stimulated from the ground state of the trap, and are subsequently transported either into the excited state of the trap, or to a band-tail, extending below the high mobility edge of the conduction band, from which they can either get re-trapped, or they can recombine with holes by a quantum tunneling process [6]. According to Poolton et al. [7], the trap depth E of feldspars has been calculated around 2 eV, or even higher. This means that by stimulating the trap with blue light (470 nm) in which the energy is around 2.63 eV, BLOSL stimulation causes both direct transitions into the conduction band as well as transitions into either the excited state or the band tails of the conduction band [6].

As far as stimulating the trap with IR light (880 nm) and energy around 1.43 eV, the possible transitions are exclusively of a localized nature, because electrons do not have the necessary energy to recombine through delocalized transitions involving the conduction band [5,7].

The use of feldspars for luminescence dating has been limited, because of a basic drawback known as athermal or anomalous fading

* Corresponding author.
E-mail addresses: vasilikiag@yahoo.gr, vaaggeli@auth.gr (V. Angeli).

https://doi.org/10.1016/j.jlumin.2020.117425
Received 12 December 2019; Received in revised form 30 May 2020; Accepted 2 June 2020
Available online 6 June 2020

(AF hereafter) [8–14]. AF is associated with quantum tunneling-induced recombination, which leads to the loss of the measurable luminescence signal after irradiation [15,16]. Quantum tunneling can arise from either the ground state, from an excited state, or from the band-tail states. However, research has shown that IRSL measurements carried out at high temperature can reduce the effects of tunneling, so that the corresponding AF effect becomes negligible [17,18]. Several researchers have concluded that athermal fading can be circumvented by applying the following techniques (a) post-IR IRSL (pIR IRSL) protocols, namely a two-step protocol involving IRSL, (b) a multiple-step protocol, which contains IRSL measurements at sequentially increasing temperatures (termed multi-elevated-temperature post-IR IRSL, or MET pIR IRSL) [17–20] and (c) radiofluorescence [21,22].

The most recent model describing the effect of athermal fading is the localized tunneling recombination (LTR) model. According to this model electron traps and luminescence centers are considered as pairs separated by a distance, which follows the nearest-neighbor distribution [23,24]. Kitis and Pagonis [24] quantified the model of Jain et al. [23], by deriving exact analytical expressions for different experimental stimulation modes. Polymeris et al. [25] have analyzed the kinetics of TL signals from feldspars.

There are very few reports in the literature concerning possible correlations among the various luminescence signals in feldspar samples. Firstly, a correlation between BLOSL and IRSL with TL was attempted by Sfampa et al. [26], for ten different K-feldspars. Later, Kitis et al. [27] showed that if a feldspar sample was stimulated using a two-step protocol (initially with IR stimulation and subsequently with blue light), the IR stimulation would influence the part of the BLOSL decay curve corresponding to the fast BLOSL component. This study was performed using the same Hoya U340 filter for the detection of both IRSL and BLOSL signals.

Recently, Angeli et al. [28] established a quantitative correlation between the IRSL signal and the tunneling component of the BLOSL signal for different geological materials, namely gypsum and fluorapatite of various grain size fractions. These authors reported that the electrons responsible for the IRSL emission, may also be responsible for the fast BLOSL components. In this study, different detection filters were used for the IRSL and BLOSL signals.

The present paper follows on directly from these two studies, and concerns the IRSL and BLOSL signals in three different K-feldspars. In fact, the present study is an extended version of the work of Kitis et al. [27]; moreover it includes two different two-step stimulation protocols. Similar to the study of Angeli et al. [28], different detection filters were used for the IRSL and BLOSL signals. Although the physics of IRSL and BLOSL phenomena are different, there are strong arguments that these stimulation modes act on the same set of trapped electrons. The complex luminescence mechanisms in feldspar samples require a detailed analysis of the complex BLOSL and IRSL signals, using a computerized deconvolution analysis. In the case of BLOSL signals, the data have been processed using a combination/superposition of tunneling and general order kinetic equations, while for the IRSL signals the processing of data was carried out using tunneling equations solely, with the details given later in this paper.

Based on this rationale, the aims of the present study are:

a. To check the validity and robustness of the deconvolution approach, for both BLOSL and IRSL signals in K-feldspar samples;
b. To understand the mechanism of BLOSL and IRSL signal production, by studying the corresponding deconvolution parameters (the lifetime of components, the dimensionless acceptor density parameter ρ' etc) of the LTR model, by using two-step stimulation protocols;
c. To investigate the possible dependence of these parameters on the structural properties of K-feldspars;
d. To attempt a correlation between the luminescence signals.

2. Experimental procedure

2.1. Samples and crystal structure

Three different potassium feldspar samples were the subject of the present study. Alkali feldspars consist of a three dimensional array of corner-sharing AlO_4 and SiO_4 tetrahedra. Three out of the four T-cation sites (representing small-sized cations mostly Si^{+4} and Al^{+3}) in their unit cell are occupied by Si-cations, while the fourth is occupied by an Al-cation. The probability of an Al-cation occupying one of the T_1 sites ($\Sigma t_1 = t_{10}+t_{1m}$) was calculated using appropriate equations [29]. According to both X-ray powder diffraction (XRPD) and Fourier Transform Infrared (FTIR) spectroscopy patterns, K-feldspars are divided in three different groups: sanidines, orthoclases and microclines. It should be noted that the Σt_1 value is lowest for the sanidine group, and highest for the microcline group, while the orthoclase group shows intermediate values. The examined samples were selected in order to cover the entire region of the potential Σt_1 values [30].

This study involves three different feldspar samples, a microcline sample (with laboratory code name ELD1), a sanidine sample (code name MRK4) and an orthoclase sample (code name VRS3). These three samples are almost identical in their physical properties, and it is impossible to distinguish between them without either XRPD or FTIR analysis. The only difference is their crystal structure, as microcline crystallizes in the triclinic system, and orthoclase and sanidine crystallize in the monoclinic system.

The feldspar samples used in this paper were included in a previous study by Polymeris et al. [30], who investigated the possibility of using TL for structural characterization for a total of ten K-feldspar samples. These authors found a good correlation between the TL sensitivity and individual K-feldspar structure, and suggested that these samples are ideal for investigating basic TL, BLOSL and IRSL signals and possible correlations among them. Two of the three samples in the present study were previously studied by Pagonis et al. [31] and Polymeris et al. [25]. However, the feldspar samples used in this paper are not the same as those studied by Kitis et al. [27]. The sample preparation was described previously in Refs. [30], and will not be repeated here.

2.2. Apparatus

All luminescence measurements were carried out using a RISØ TL/OSL reader (model TL/OSL-DA-20, Reader ID: 267 [32]) equipped with a high power blue LED light source (470 nm, FWHM 20 nm), delivering at the sample position a maximum power of 40 mW/cm^2, an infrared solid state laser (880 nm, FWHM 75 nm, maximum power 135 mW/cm^2) and a $^{90}Sr/^{90}Y$ beta particle source, delivering a nominal dose rate of 0.1083 Gy/s. An EMI 9235QB photomultiplier tube was used for the detection of all luminescence signals. For the case of blue OSL measurements, a Hoya (U-340) filter was used for light detection (340 nm, FWHM 80 nm). For IRSL, the conventional, most commonly used filter combination of the 2 mm Schott BG 39 and the 4 mm Corning 7–59 (known as the blue filter pack) was used for detection of blue emission in feldspars [20]; this latter combination was used, since in the present study only blue stimulated OSL was studied [6]. All measurements were performed in a nitrogen atmosphere with a low constant heating rate of 2 °C/s, in order to decrease the temperature gradient between the sample and the sample holder [33], and the samples were heated up to the maximum temperature of 500 °C. A test dose of 50 Gy was used for all samples.

2.3. Experimental protocols

Two different two-step protocols were used in the framework of the present study, involving a combination of IR and blue light stimulation. The difference between the two protocols is which of these two stimulations is applied first. Such a comparison of the two-step protocols is

applied for the first time in the literature.

In the first two-step experimental protocol, IR stimulation is applied first for various stimulation times t_i, followed by the blue light stimulation for a fixed time interval of 1 ks. The experimental procedure used is as follows:

Step 1: Test dose (50 Gy)
Step 2: CW- IRSL at the continuous wave mode for time t_i (initial stimulation, denoted as the IRSL signal in the rest of the paper)
Step 3: Residual blue CW-OSL for 1000 s (denoted as post-IR BLOSL in the rest of this paper)
Step 4: Measurement of Residual TL signal
Step 5: Repeat steps 1–4 for another time t_i in step 2

The stimulation times used in step 2 of the first protocol are 0, 5, 10, 25, 35, 50, 75, 100, 250 and 500 s.

The second two-step protocol includes the following steps:

Step 1: Test dose (50 Gy)
Step 2: CW-OSL stimulation for time t_i (initial stimulation, denoted as BLOSL signal in the rest of the paper)
Step 3: CW-IR stimulation for 300 s, measuring the Residual IRSL signal (denoted as post-BL IRSL in the rest of this paper)
Step 4: Measurement of Residual TL signal
Step 5: Repeat steps 1–4 for a different stimulation time t_i in step 2.

The stimulation times used in step 2 of the second protocol are 1, 2, 4, 8, 16, 30, 50 and 100 s.

These two protocols were carried out in a single aliquot mode for the three feldspars samples. This makes it necessary to test for sensitization, or sensitivity changes following consecutive cycles of irradiation and heating [27,31]. However, no sensitivity changes were detected for the luminescence signal of feldspars [25,31]. Finally, it is noted that a similar two-step protocol was used by Sfampa et al. [34], and included an isothermal TL and a residual IRSL stimulation.

2.4. Methods of analysis

Taking into consideration that recombination can take place via both localized and de-localized transitions, a computerized curve deconvolution analysis was used which includes two different analytical equations.

The first equation is based on general order kinetics (GOK hereafter) [35,36], to describe a delocalized transition through the conduction band:

$$I(t) = I_o\left[1 + \frac{(b-1)t}{\tau}\right]^{-b/(b-1)} \quad (1)$$

where $I(t)$ is the intensity of luminescence signal as a function of time, I_0 is the initial luminescence intensity, τ is the component lifetime and b is the order of kinetics which is allowed to vary between 1.001 and 2.05.

The second equation is the analytical equation of Kitis and Pagonis [24], which is based on the LTR model of Jain et al. [23]; the probability of tunneling in this model varies with the donor–acceptor distance. According to this model, trapped electrons are raised to a higher energy level, from which they can tunnel to the nearest neighbor luminescence center. In this manner, the electrons recombine with holes and light is emitted. The analytical equations are:

$$I(t) = 3n_o\rho' z F(t)^2 \frac{1}{1+zt}\exp\left(-\rho' F(t)^3\right) \quad (2)$$

$$F(t) = \ln\left(e + \frac{zt}{\tau_{tun}}\right) \quad (3)$$

$$\tau_{tun} = (\sigma\,\phi)^{-1} \quad (4)$$

where $I(t)$ is luminescence intensity as a function of time t; n_o is the initial concentration of the donors; $z = 1.8$ is a constant; τ_{tun} is the tunneling luminescence lifetime for recombination processes taking place via the excited state; ρ' is a dimensionless parameter representing the constant acceptor density; σ is the photo-ionization cross section, and ϕ the stimulation flux. Equations (2)–(4) were used for the analysis of the localized (tunneling) components.

All curve fittings were performed using the software package *Microsoft Excel*, with the *Solver* utility [37], while the goodness of fit was tested using the Figure Of Merit (FOM) of Balian and Eddy [38] given by:

$$FOM = \sum_i \left[\frac{Y_{exper} - Y_{fit}}{A}\right] \quad (5)$$

where Y_{exper} is the experimental data, Y_{fit} is the fitted data and A is the area of the fitted curve.

3. Results and discussion

3.1. Bleaching effects on the OSL and IRSL decay curves

In the framework of the first protocol, blue light stimulation follows IR stimulation; thus we measure the IRSL signal followed by post-IR BLOSL. Fig. 1 presents a selection of the post-IR BLOSL curves for different IRSL stimulation times (0, 35, 100 and 500s), and for all three feldspars (Fig. 1**a**, **c** and **1e**). According to these plots, the IRSL stimulation has a minor effect on the measured post-IR BLOSL signal, with the effect visible only for stimulation times up to 100s; for higher IR stimulation times, the change in the decay curve is negligible. This feature suggests that the IRSL stimulation does not influence the entire post-IR BLOSL decay curve, but only the component that decays faster. Similar experimental features were also presented in Ref. [27], for different feldspars samples, as well as by Angeli et al. [28] for both apatite and gypsum samples.

In the second protocol, the feldspars were exposed initially to a blue stimulation, followed by measurement of the post-BL IRSL decay curves. Fig. 1**b**, **d** and **1f** present a selection of these post-BL IRSL curves, for 4 different BLOSL stimulation times of 0, 8, 30 and 100 s. These figures show clearly that the BLOSL stimulation influences the post-BL IRSL signal throughout the post-BL IRSL curve. As the OSL stimulation increases, the entire post-BL IRSL curve is shifted to lower intensities; the intensities of the total post-BL IRSL curve (**plots b, d** and **f**) are two orders of magnitude lower than the corresponding intensities of the post-IR BLOSL curves (**plots a, c, e**), according to the second and first protocol respectively. In other words, stimulation using blue light affects *both* components of the post-BL IRSL curves.

An additional effect seen in Fig. 1**b**, **d** and **1f,** is that in all cases the post-BL IRSL curves do not have the usual monotonically decaying shape. Instead, the post-BL IRSL curves include an initially increasing part for the first few seconds of stimulation, followed by the expected decaying part. This type of non-monotonic behavior has been reported for complex IRSL measurements at higher temperatures, such as the pIR IRSL or MET pIR IRSL protocols. Recently, similar IRSL decay shapes were reported by Şahiner et al. [20,39] for pure K-feldspar samples recovered from igneous rocks of Northern Greece [30] and from Sakarya, Turkey, respectively. This is the first time in the literature that similar shapes are reported for IRSL measurements carried out at room temperature.

3.2. Number of components

Fig. 2 shows an example of the deconvolution analysis (on sample ELD1) for the different signals measured in both two-step protocols,

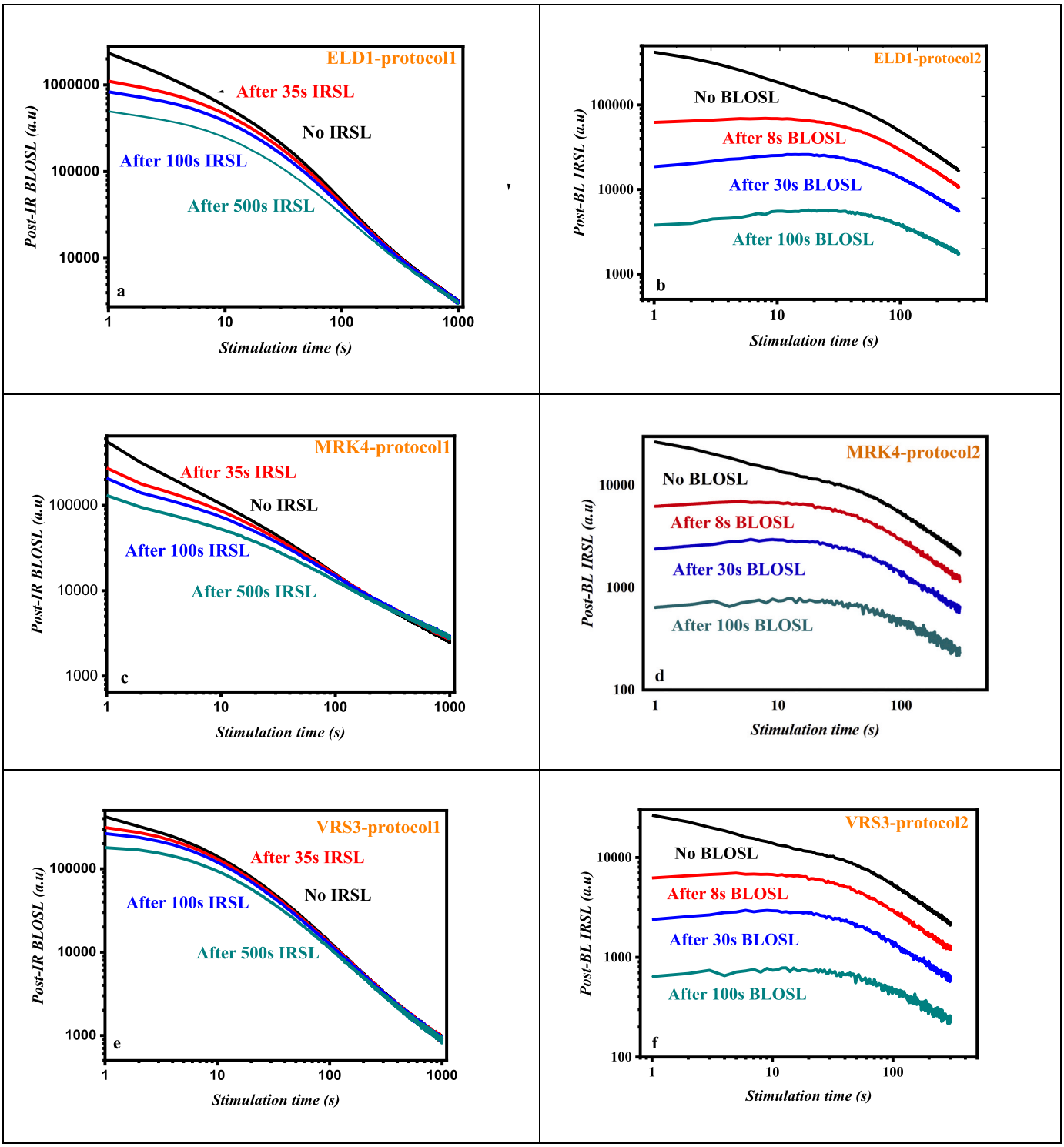

Fig. 1. (a), (c), (e) Post-IR BLOSL decay curves for ELD1, MRK4 and VRS3, obtained after IRSL bleaching for 0s (unbleached sample), 35s, 100s and 500s in the first two-step protocol. **(b), (d), (f):** Post-BL IRSL decay curves for ELD1, MRK4 and VRS3, obtained after blue light bleaching for 0s (unbleached sample), 8s, 30s and 100s in the second two-step protocol.

namely IRSL/post-IR BLOSL for the first protocol, and BLOSL/post-BL IRSL for the second protocol. Two components were required for a satisfactory fitting during the deconvolution analysis of all decay curves, and for all three feldspars. Specifically, for the BLOSL and post-IR BLOSL stimulations, the components used include one tunneling and one GOK component. These components are hereafter called C_{BLOSL_tun} and C_{BLOSL_GOK} as well as $C_{post\text{-}IR\ BLOSL\ \_tun}$ and $C_{post\text{-}IR\ BLOSL\ \_GOK}$ respectively.

As it becomes obvious from Fig. 2, both C_{BLOSL_GOK} and $C_{post\text{-}IR\ BLOSL\ \_GOK}$ components have long lifetimes, much larger than the corresponding lifetimes of the tunneling components. The GOK component is a long term component which requires prolonged bleaching times in order to decay substantially. In addition, the lifetime τ of these GOK components is found to be independent of the various stimulation times used during the IRSL stimulation step of the protocol.

It is worth emphasizing that deconvolution analysis of BLOSL signal was also attempted using just two GOK components. In the framework of

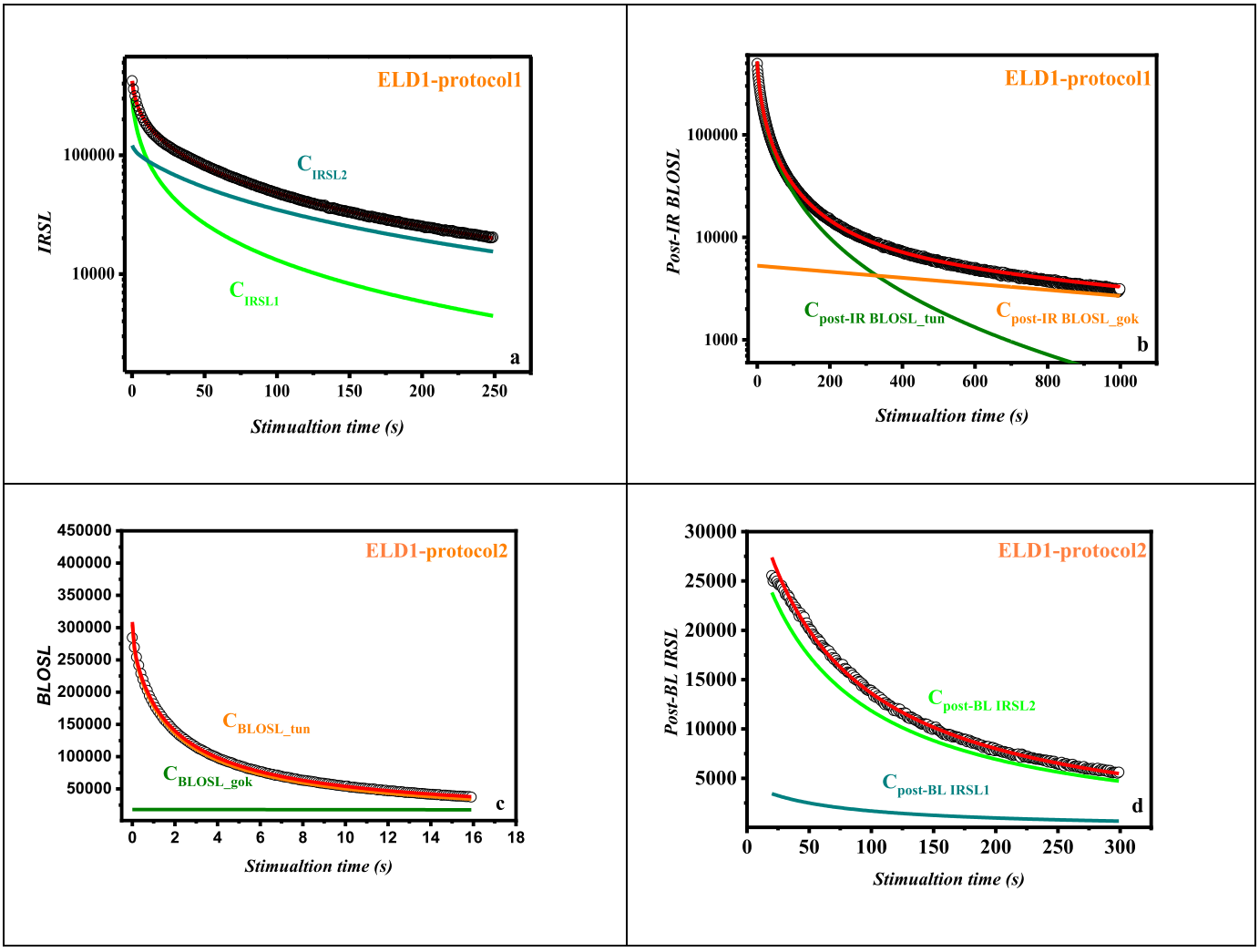

Fig. 2. Deconvolution examples of decay curves for the case of ELD1 feldspar sample. **(a), (b)**IRSL and post-IR BLOSL decay curves from protocol 1, as a function of stimulation time. **(c), (d)** BLOSL and post-BL IRSL decay curves from protocol 2, as a function of stimulation time. Experimental data are presented as unfilled dots, while GOK and tunneling components and their sum are presented as continuous lines.

such analysis, the results indicated that the lifetime of the fast GOK BLOSL component increases with increasing stimulation time. This latter result is rather remarkable, if we consider that the temperature and all the experimental conditions remain the same. This is another indication of the existence of tunneling effects inside the crystal structure of all the three K-feldspars. These results stand in good agreement with those reported by Kitis et al. and Angeli et al. [27,28] respectively.

On the other hand, each of the IRSL and post-BL IRSL curves measured according to both experimental protocols, requires two *tunneling* components for an acceptable fit. The number of components used here stands in good agreement with previous reports [20,26–28, 40]. Hereafter, these IRSL/post-BL IRSL components will be referred to as C_{IRSL1}, C_{IRSL2} and $C_{post\text{-}BL\ IRSL1}$, $C_{post\text{-}BL\ IRSL2}$ respectively. Fig. 2 shows that the decay of these two components depends strongly on the stimulation time used in **step 2** of −the protocols. In both IRSL and post-BL IRSL curves, the first component is the dominant one, while the second IRSL component is quite faint in intensity. The FOM value for the analysis of all samples and for both protocols was less than 2%, indicating a good fit to the experimental data.

3.3. Results for the parameters τ, ρ' of the LTR model

3.3.1. Lifetimes of tunneling components of all signals

Following the deconvolution analysis described above, Fig. 3 presents the dependence of the lifetime of each tunneling component, on the duration of the initial stimulation in **step 2** of the two protocols. Each plot of Fig. 3 corresponds to a different feldspar sample, and consists of six curves. Four curves represent the lifetimes of the two tunneling IRSL components for both protocols, while the remaining two curves represent the lifetimes of the tunneling BLOSL component. Following the nomenclature of the previous section, the lifetimes of BLOSL tunneling components are termed hereafter as τ_{BLOSL_tun} and $\tau_{post\text{-}IR\ BLOSL\_tun}$ for the second and first protocol respectively, while the lifetimes of the tunneling IRSL and post-BL IRSL components are termed as τ_{IRSL1}, τ_{IRSL2} according to the first protocol,and $\tau_{post\text{-}BL\ IRSL1}$, $\tau_{post\text{-}BL\ IRSL2}$ according to the second experimental protocol.

As Fig. 3 shows, all tunneling lifetimes increase systematically with the stimulation time of **step 2** in both protocols. In some cases, plateaus are also formed at prolonged stimulation times. This latter feature stands in good agreement with the corresponding behaviour reported by Kitis et al. [27]. This increase of the tunneling lifetime parameter can be interpreted within the LTR model, as follows: as the stimulation time in **step 2** is increased for both protocols, pairs of electrons and positive charges corresponding to shorter distances recombine first, and only more distant pairs remain in the system. These larger tunneling distances lead to an increase of the effective tunneling recombination lifetime. It is worth mentioning that in both protocols, the second components of all post-BL IRSL signals are of low intensity, and the first

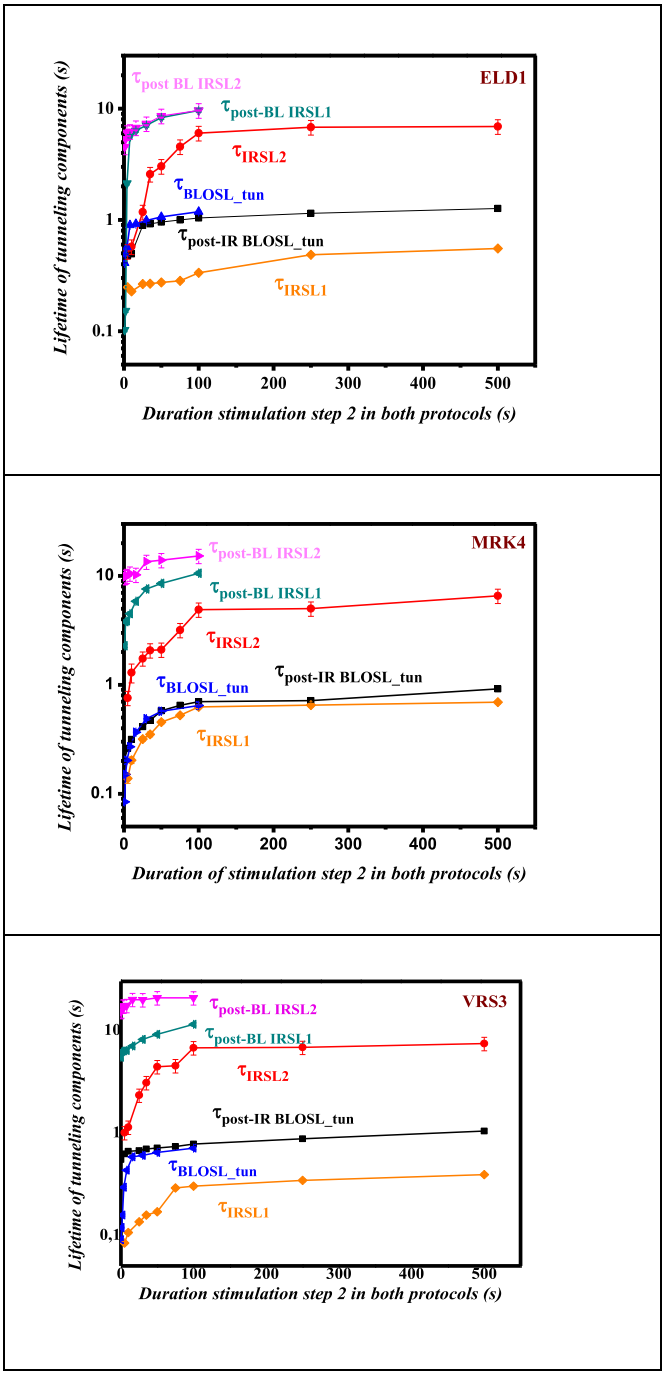

Fig. 3. The lifetimes of each tunneling component are presented for the ELD1, MRK4 and VRS3 samples, as a function of the duration of the initial stimulation in step 2 of both protocols. The nomenclature is explained in detail in section 3.3.1. Note the logarithmic y-axis.

post-BL IRSL component is the dominant one. Consequently, due to this low intensity, the errors of the corresponding tunneling recombination lifetimes are quite enhanced.

A notable feature of Fig. 3 concerns the tunneling recombination lifetimes of the consecutive-sequential stimulation modes. Specifically the lifetime parameter of the first stimulation mode always yields lower values than the tunneling recombination lifetimes corresponding to the respective residual signals. As recombination is a stochastic process, it is likely to occur anywhere and the proximity of a recombination centre does not mean that recombination will be restricted only to a limited area. Nevertheless, Fig. 3 provides evidence supporting the idea that the first stimulation o **step 2** takes mostly advantage of the closest pairs of donors and acceptors, while the second stimulation of **step 3** can take advantage of more distant charge pairs. This feature is valid independently of the stimulation sequence. Similar conclusions were also reported by Şahiner et al. [20] for IRSL, post-IR IRSL and MET pIR IRSL signals measured at various combinations of temperatures, as well as by Sfampa et al. [34] for IRSL and ITL signals.

However, it is quite important to note two more features of entire Fig. 3:

i) The recombination lifetimes of the tunneling component for both BLOSL (blue triangles) and post-IR BLOSL (black squares) signals are the same, independent on whether the blue stimulation mode is applied first or not. These lifetimes are unaffected by the order of the two stimulations in the protocols.
ii) The recombination lifetimes of the post-BL IRSL signals in protocol 2 yield the largest values of all signals; this is the case for all potassium feldspars that were the subject of the present study.

During BLOSL stimulation, a conduction band recombination process has a measurable probability and the outcome of the blue stimulation is the same, independent of whether infrared stimulation precedes it, or not. This is the reason why for both protocols, the tunneling components of both BLOSL and post-IR BLOSL signals yield identical recombination lifetimes. Of course, in the case where the infrared stimulation follows the blue light stimulation, the post-BL IRSL components yield much higher lifetimes, as the electrons travel longer distances in order to find positive charges and recombine.

Fig. 4 presents the recombination lifetimes for a selection of tunneling components, for all three K-feldspars, for the post-IR BLOSL tunneling component (**plot a**), as well as for the dominant $C_{\text{post-BL IRSL1}}$ and C_{IRSL1} components of the IRSL signals (**plots b** and **c**, respectively). As the post-IR BLOSL and BLOSL analyses yield almost identical values of this parameter, only one plot is presented.

An important conclusion from Fig. 4 is the possible dependence of the tunneling component lifetimes on the crystal structure. Specifically, this dependence is seen for $\tau_{\text{BLOSL\_tun}}$, $\tau_{\text{post-IR BLOSL\_tun}}$ and $\tau_{\text{post-BL IRSL1}}$. According to Fig. 4, in the K-feldspar with the largest cell unit volume, namely ELD1 (719.45 Å^3), the electrons travel for longer times before recombination, while in the MRK4 which corresponds to the lowest unit cell volume (711.92 Å^3) the electrons travel for shorter times before recombining [34]. In the ELD1 sample with the largest unit cell volume, electrons must travel larger distances (and for longer times) [41]. Similar experimental results are presented in Fig. 4**b**, although the correlation between the lifetime of the tunneling components and the crystal structure is not so clear.

On the other hand, Fig. 4**d** shows that no apparent correlation was found between the crystal structure and the tunneling post-BL IRSL component 2 ($\tau_{\text{post-BL IRSL2}}$). The lifetime of this component seems to be independent of the crystal structure. A safe conclusion cannot be reached with this data, possibly due to the large error in the values of the lifetime of this second component.

3.3.2. *The dimensionless density parameter ρ'*

According to the LTR model of Jain et al. [23], the concentration of acceptors in feldspars is much larger than the concentration of electrons, and therefore one expects that the dimensionless density of acceptors ρ' would stay constant throughout the experiment. This dimensionless density is the second important parameter (besides the lifetimes), which is extracted by the deconvolution of the various signals in this paper.

The donor-acceptor density was discussed only in a limited number of works. Şahiner et al. [20] have reported that in their IRSL, post-IR IRSL and MET pIR IRSL signals, the values of the ρ' parameter for each luminescence component are constant, and that the ρ' values are independent of the stimulation temperature. In these types of experiments the density parameter yields a consistent Gaussian distribution.

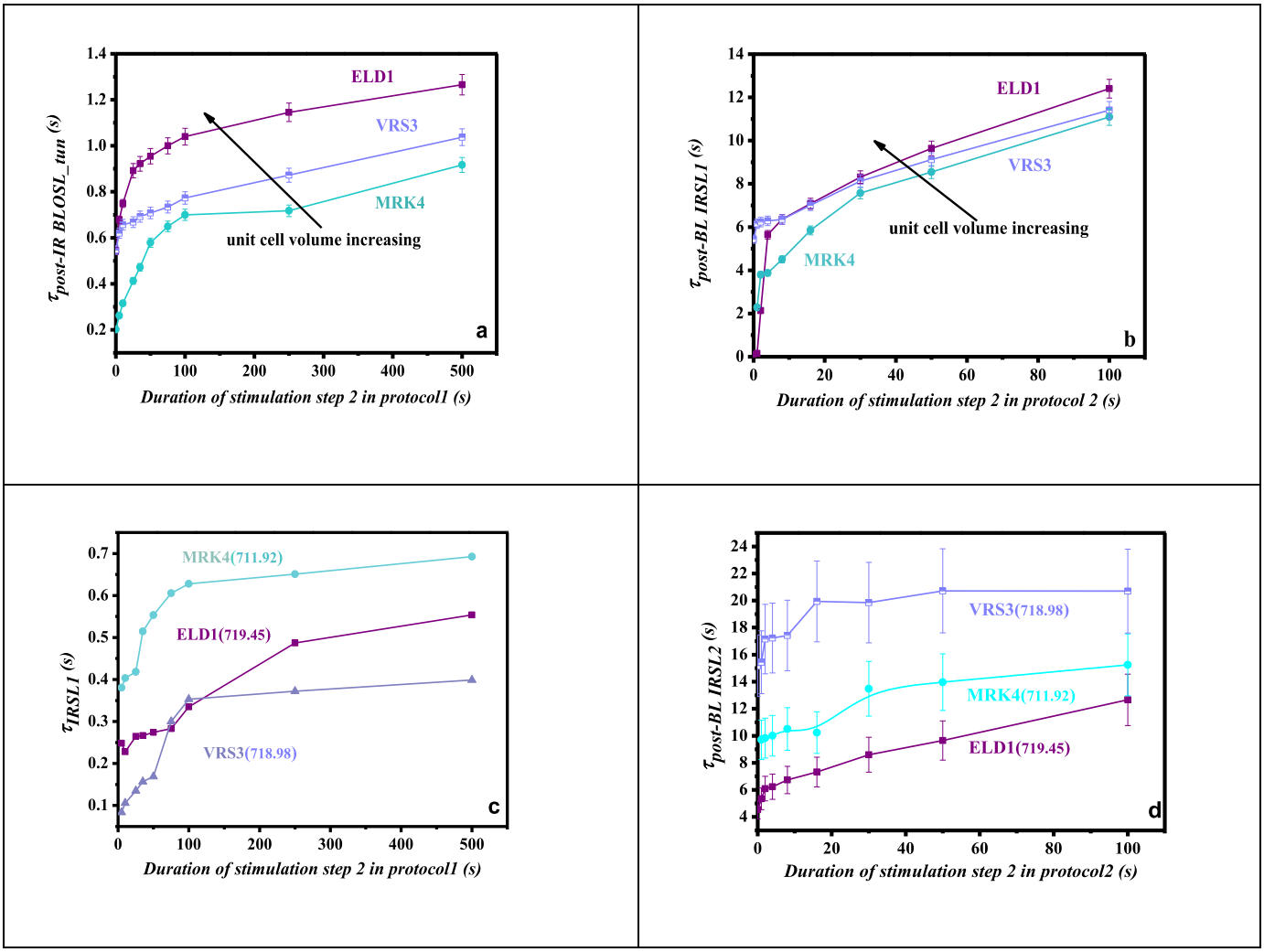

Fig. 4. The recombination lifetimes of the tunneling components for all three K-feldspars for the post-IR BLOSL tunneling component (**plot a**), as well as the components $C_{post\text{-}BL\ IRSL1}$, C_{IRSL1} and $C_{post\text{-}BL\ IRSL2}$ of the IRSL signals (**plots b, c** and **d** respectively), as a function of the initial stimulation time. **Plots a** and **b** indicate a correlation between the lifetimes of these tunneling components and the crystal structure of these feldspars, while **plots c** and **d** are characteristic examples for the absence of any similar correlation.

However, as the number of consecutive stimulations is increased, as in the MET pIR IRSL protocols, these Gaussian distributions became quite wide and formed rather scattered histograms. Recently Sfampa et al. [34] also reported values of ρ' parameter which are independent of the stimulation temperature, for both IRSL and ŦTL signals. It is quite important to note that in both of these two previous studies, the only parameter that changed experimentally was the stimulation temperature, while the duration of the stimulation duration was kept fixed.

Fig. 5**a** and **b** presents the dependence of the dimensionless parameter ρ', on the initial stimulation of the two-step protocols. The parameters are denoted by ρ'_{IRSL1} and, ρ'_{BLOSL_tun} for the first and second protocol, respectively. As the stimulation duration increases in both protocols/stimulation modes, so does the value of the dimensionless parameter ρ'. Throughout the entire range of stimulation duration in **step 2**, the values of the parameter ρ' increase smoothly and not abruptly, while plateaus are also formed at extended stimulation times. Moreover, as Fig. 5**a** and **b** shows, these increasing ρ' values depend on the unit cell volume of the feldspar sample. In addition, this dependence is different for the ρ'_{IRSL1} and ρ'_{BLOSL_tun} parameters; the former parameter is decreasing with increasing stimulation duration, while the latter increases.

On the contrary, for the case of the second (residual) signal measured in **step 3** of both protocols, analysis of both post-BL IRSL and tunneling post-IR BLOSL components yield a stable value of the ρ' parameter, which is independent of the duration of the prior stimulation. Fig. 5**c** and d presents the average values of the $\rho'_{post\text{-}IR\ BLOSL\_tun}$ and $\rho'_{post\text{-}BL\ IRSL1}$ components for the first and second protocol respectively, plotted versus the unit cell volume of the K-feldspars. The errors shown correspond to 1σ over the average value. Fig. 5**c** also contains the results of Kitis et al. [27], obtained with a similar analysis of four additional K-feldspars.

The insets of Fig. 5**c** and **d** present examples of histograms of the corresponding acceptor density. Each histogram is accompanied by the corresponding Gaussian distribution presented as a solid line, as was done by Şahiner et al. [20]. Note the very narrow Gaussian distributions.

The combined data from the two different studies indicate that the values of the $\rho'_{post\text{-}IR\ BLOSL\_tun}$ parameter fall clearly in three groups, each one corresponding to the groups of sanidines, orthoclases and microclines. In other words, the values of these parameters are clearly correlated to the crystal structure of the K-feldspar. On the contrary, the three values of the parameter $\rho'_{post\text{-}BL\ IRSL1}$ reported here seem independent of the crystal structure. Moreover, it becomes obvious from Fig. 5 that the second stimulation yielding the residual signal, gives larger values of ρ'. Similar results were also reported by Şahiner et al. [20]; Kitis et al. [27] and Sfampa et al. [34], in their two-step stimulation protocols. Finally, it is worth mentioning that all values of ρ' reported in all these studies do not exceed a maximum of $\rho' \approx 0.01$.

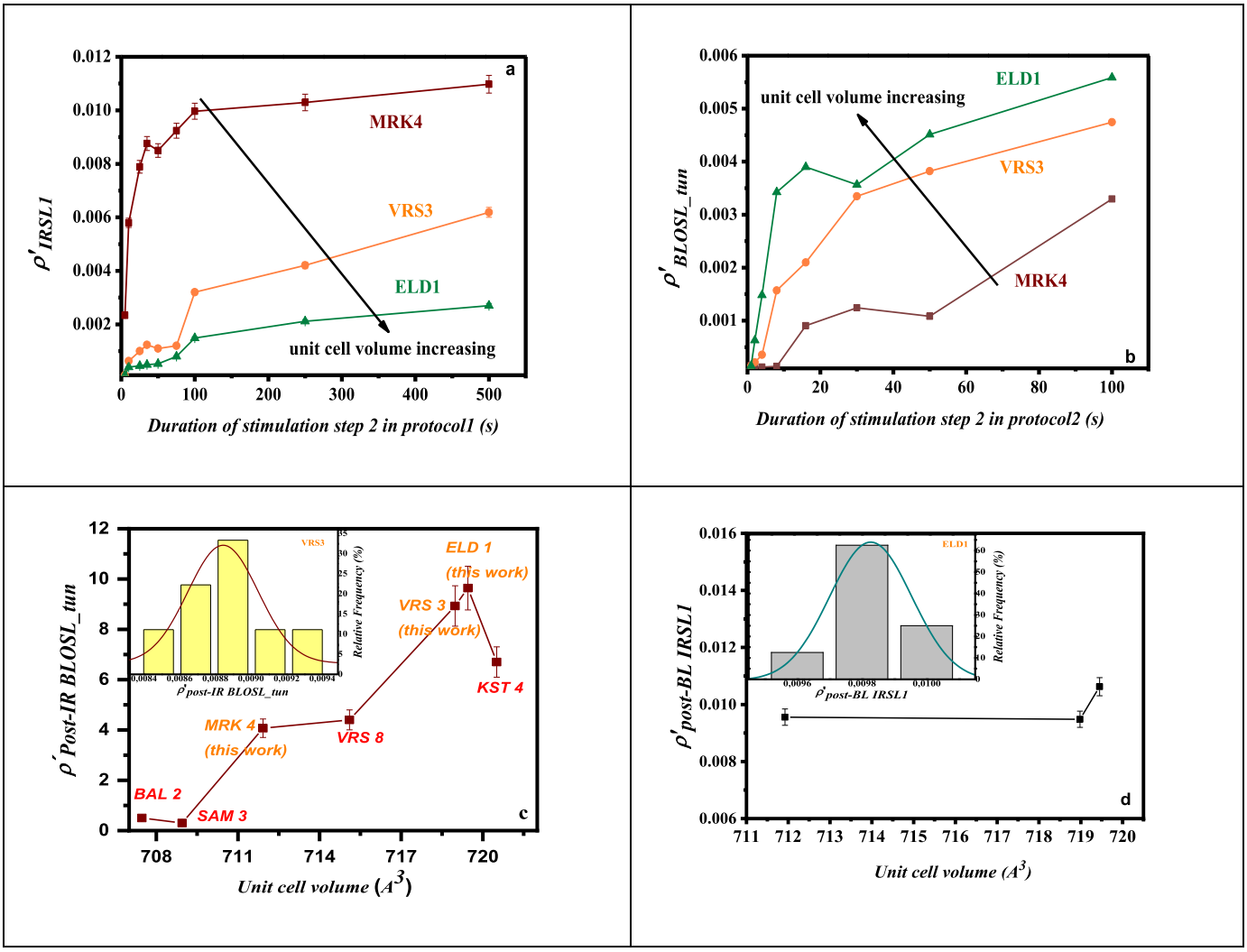

Fig. 5. (a),(b): The dimensionless density parameter ρ'_{IRSL1} and $\rho'_{BLOSL\ tun}$ as a function of the initial stimulation of step 2 in both protocols. **(c), (d)** The average values of $\rho'_{post\text{-}IR\ BLOSL\_tun}$ and $\rho'_{post\text{-}BL\ IRSL1}$ plotted versus the unit cell volume of the corresponding K-feldspars. Fig. 5**c** includes also the results from Kitis et al. (2016). The insets of show the data in the form of a histogram.

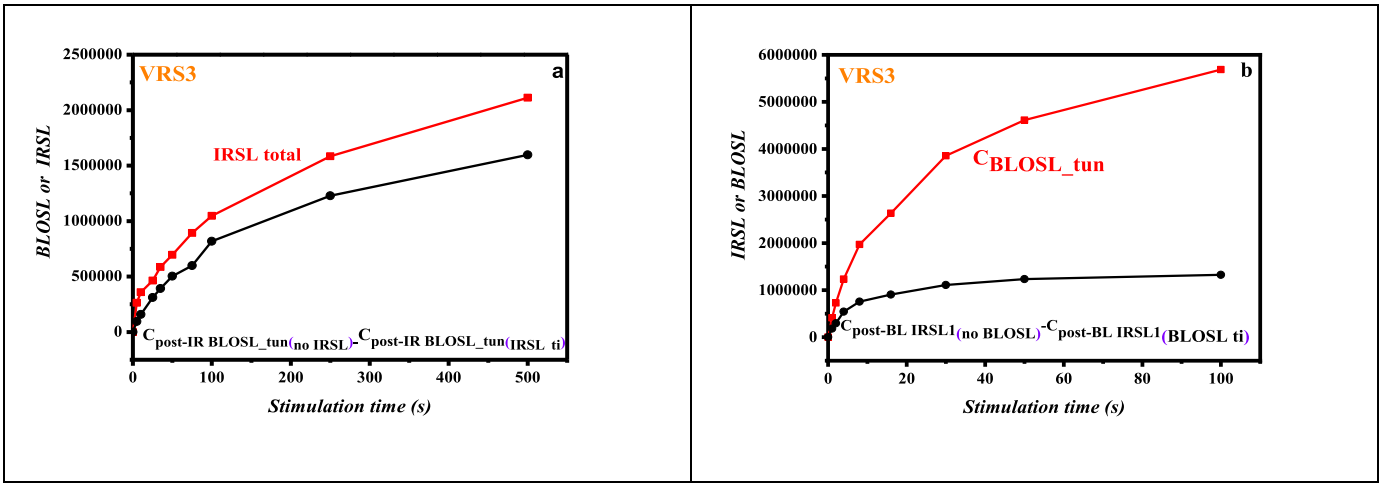

Fig. 6. (a) Comparison between the total integrated IRSL signal and the variation of the intensity of the $C_{post\text{-}IR\ BLOSL\_tun}$ for various IRSL stimulation time. **(b)** Comparison between the total integrated tunneling component of the BLOSL signal and the variation of the intensity of the $C_{post\text{-}BL\ IRSL1}$ component, for various OSL stimulation times.

3.3.3. Component resolved intensities

The previous studies of Kitis et al. [27] and Angeli et al. [28], contained only the first protocol of the present study. Both of these studies reported a qualitative correlation between the fast OSL component and the first IRSL component. This conclusion is also confirmed in the present study, according to Fig. 1 **a,c,e** and also shown in Fig. 6**a**. This latter figure presents a comparison between the total integrated IRSL signal and the variation of the intensity of the $C_{post\text{-}IR\ BLOSL\_tun}$ component, for various IRSL stimulation times in the first two-step protocol. It becomes obvious that the two curves lie very close to each other, indicating a connection between the IRSL signal and the fast BLOSL component. Since these two signals seem to be correlated both qualitatively and quantitatively, it is possible that this fast BLOSL component in feldspars is also a tunneling component.

Fig. 6**b** presents a comparison between the total integrated tunneling component of the BLOSL signal and the variation of the intensity of the $C_{post\text{-}BL\ IRSL1}$ component, for various BLOSL stimulation times in the second two-step protocol. It is evident that the tunneling BLOSL component could also be related quantitatively to the $C_{post\text{-}BL\ IRSL2}$ component. Fig. 6 shows results only for the VRS3 sample, however similar results were also obtained for the other two feldspar samples.

Fig. 7 presents the total integrated intensity versus the stimulation time, for both signals and for both protocols, i.e. IRSL/post-IR BLOSL for the case of protocol 1, and BLOSL/post-BL IRSL for the case of protocol 2. This figure shows that the total signal for the ELD1 sample (microcline), is much more intense by almost one order of magnitude than the corresponding integrated intensities for the other two samples. This conclusion is independent of the stimulation modulus (blue light or IR). Furthermore, the total integrated signals for the sanidines and orthoclases are of comparable total intensities. These results are in good agreement with those reported by Sfampa et al. [26], for 10 different K-feldspar samples. These authors have indicated that for their two step protocols, the total integrated intensities of IRSL, BLOSL and Residual TL after BLOSL or IRSL signals are higher for microclines, and almost identical for sanidines and orthoclasts. Similarly, the residual levels after bleaching are lower for the cases of microclines.

The results of this study are also in agreement with those of Sfampa et al. [26], who reported that microcline samples yield faster bleaching rates, while sanidines are less affected by bleaching. In this study only the intensity of the GOK component of the post-IR BLOSL signals indicates a correlation with the structural features of the K-feldspar samples. The data for the other two groups of samples are not consistent enough to draw final conclusions.

4. Conclusions

It was observed that the lifetimes of the various components are independent of both the protocol and the stimulation sequence. Specifically, the first stimulation in the two-step protocols takes place with nearby electron-hole pairs, while in the second stimulation, the electrons have to travel longer distances, in order to find positive charges and recombine, resulting in higher lifetimes. Also, according to the

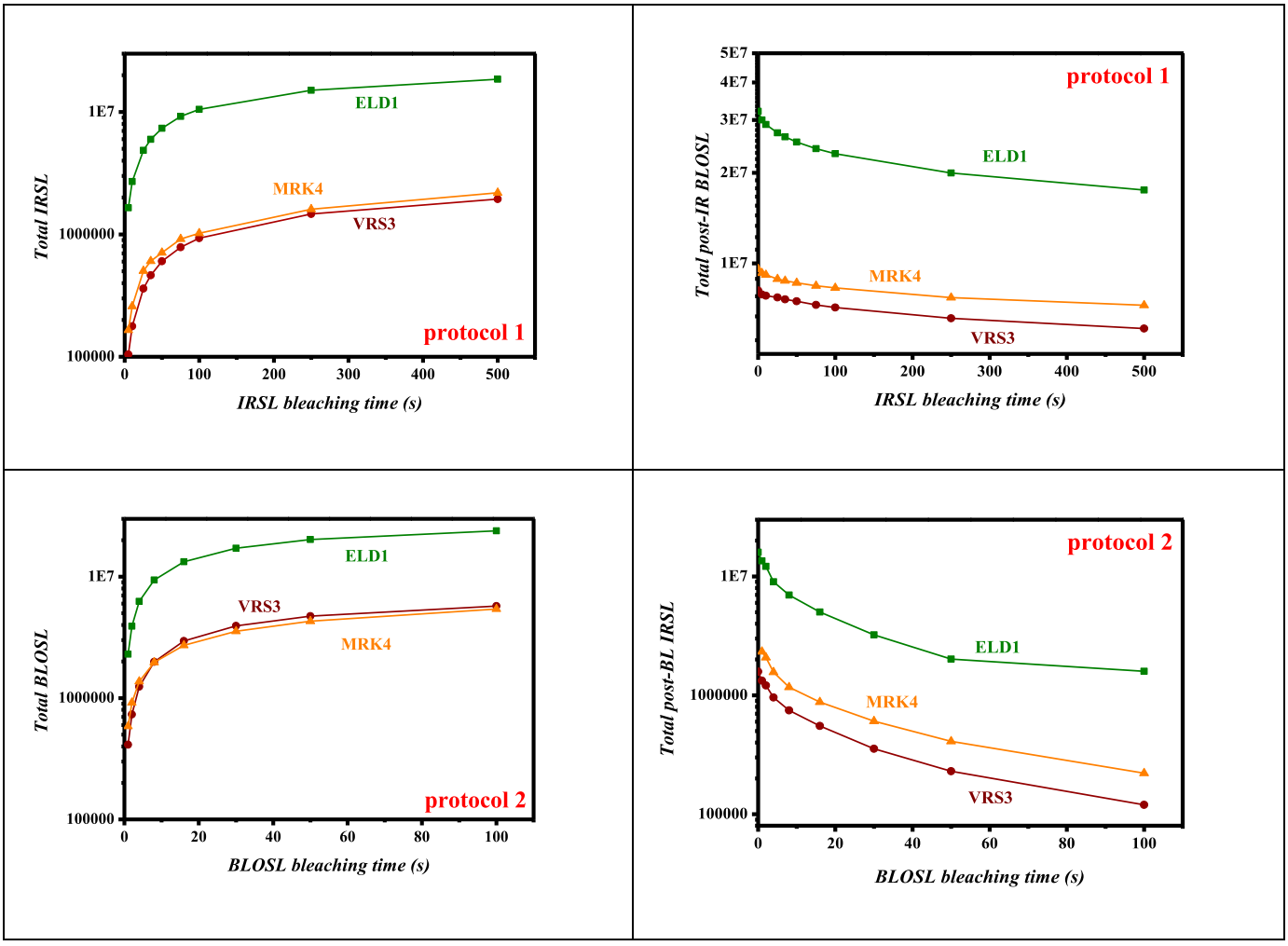

Fig. 7. (a), (b) Integrated IRSL and post-IR BLOSL signals versus the stimulation time (protocol 1). **(c), (d)** Integrated BLOSL and post-BL IRSL signals versus the stimulation time (protocol 2). A dependence of the intensity on the unit cell volume, and thus on the structure/type of the K-feldspars is apparent.

results from the first protocol (IR followed by blue light), the first IRSL component has the shorter lifetime, while the second component has the longer one. However, the results from the second protocol (blue light followed by IR), indicate that the post-BL IRSL components have longer lifetimes from the corresponding post-IR BLOSL tunneling component of the first protocol. A notable exception is noted for the blue stimulation, which yields the same recombination lifetimes of the tunneling component, irrespective of whether the BLOSL mode is first or second in the stimulation sequence.

The dimensionless density parameter ρ' seems to remain independent of the protocol and of the stimulation sequence. Based on the above, this parameter shows the lowest values in the first stimulation and not on the respective residual signal, according to the first and the second protocol.

Finally, it seems that several of the parameters depend on the crystal structure of the K-feldspars. Specifically, as presented in Fig. 4, the tunneling component lifetimes are related with the crystal structure and this correlation is stronger in the case of τ_{BLOSL_tun}, $\tau_{post\text{-}IR\ BLOSL\_tun}$ and $\tau_{post\text{-}BL\ IRSL1}$. On the other hand, the dimensionless density parameter ρ' shows a clear dependence through the unit cell volume. On the contrary, the parameter $\rho'_{post\text{-}BL\ IRSL1}$ seems to be independent of the crystal structure.

Author contributions

PhD Candidate Vasiliki Angeli: Visualization, Writing - Original Draft, Formal Analysis. **Professor George Kitis:** Conceptualization, Writing - Review & Editing, Methodology, Resources, Supervision. **Professor Vasilis Pagonis:** Software, Writing - Review & Editing, Methodology, Validation, Formal Analysis. **Professor Georg**ios **S. Polymeris:** Conceptualization, Writing - Review & Editing, Investigation, Writing-Original Draft, Validation.

Declaration of competing interest

The authors declare that they have no known competing financial interests or personal relationships that could have appeared to influence the work reported in this paper.

Acknowledgements

The corresponding author (V.A.) wants to thank Dr. Eleni Theodosoglou and Professor K.M. Paraskevopoulos for giving her the permission to use the K-feldspar samples needed for this framework.

References

[1] A.E.R. Malins, N.R.J. Poolton, F.M. Quinn, O. Johnsen, P.M. Denby, J. Physics D-applied Physics 37 (2004) 1439e1450.
[2] G.A.T. Duller, A.G. Wintle, Nucl. Tracks Radiat. Meas. 18 (1991) 379–384.
[3] G.A.T. Duller, J. Phys. D Appl. Phys. 28 (1995) 1244–1258.
[4] M.R. Krbetschek, J. Goetze, A. Dietrich, T. Trautmann, Radiat. Meas. 27 (1997) 695–748.
[5] N.R.J. Poolton, R.H. Kars, J. Wallinga, A.J.J. Bos, J. Phys. Condens. Matter 21 (2009) 485e505.
[6] M. Jain, C. Ankjaergaard, Radiat. Meas. 46 (2011) 292–309 (2011).
[7] N.R.J. Poolton, J. Wallinga, A.S. Murray, E. Bulur, L. Botter-Jensen, Phys. Chem. Miner. 29 (2002) 210–216.
[8] R. Visocekas, Nucl. Tracks 10 (1985) 521.
[9] R. Visocekas, Nucl. Tracks Radiat. Meas. 21 (1993) 175–178.
[10] R. Visocekas, N.A. Spooner, A. Zink, P. Blanc, Radiat. Meas. 23 (1994) 371–385.
[11] R. Visocekas, G. Guerin, 2006, Radiat. Meas. 41 (2006) 942–947.
[12] N.C. Tsirliganis, G.S. Polymeris, G. Kitis, V. Pagonis, J. Lumin. 126 (2007) 303–308.
[13] D.J. Huntley, M. Lamothe, J. Can, Earth Sci. 38 (2001) 1093e1106.
[14] E. Şahiner, N. Meriç, G.S. Polymeris, Radiat. Meas. 68 (2014) 14–22.
[15] A.G. Wintle, J. Lumin. 15 (1977) 385–393.
[16] R. Visocekas, V. Tale, A. Zink, N.A. Spooner, I. Tale, Radiat. Protect. Dosim. 66 (1996) 391–394.
[17] K.J. Thomsen, A.S. Murray, M. Jain, L. Bøtter-Jensen, Radiat. Meas. 43 (2008) 1474–1486.
[18] B. Li, Radiat. Meas. 45 (2010) 757–763.
[19] J.P. Buylaert, A.S. Murray, K.J. Thomsen, M. Jain, Radiat. Meas. 44 (2009) 560–565.
[20] E. Şahiner, G. Kitis, V. Pagonis, N. Meric, G.S. Polymeris, J. Lumin. 188 (2017) 514–523.
[21] M.R. Krbetschek, T. Trautmann, A. Dietrich, W. Stolz, Radiat. Meas. 32 (2000) 493e498.
[22] G. Erfurt, M.R. Krbetschek, Ancient TL 21 (2003) 35e42.
[23] M. Jain, B. Guralnik, M.T. Andersen, J. Phys. Condens. Matter 24 (2012) 85402.
[24] G. Kitis, G.S. Polymeris, V. Pagonis, N.C. Tsirliganis, Radiat. Meas. 49 (2013) 73–81.
[25] G.S. Polymeris, V. Pagonis, G. Kitis, Radiat. Meas. 97 (2017) 20–27.
[26] I.K. Sfampa, G.S. Polymeris, V. Pagonis, E. Theodosoglou, G. Kitis, Nucl. Instrum. Methods Phys. Res. Sect. B Beam Interact. Mater. Atoms 359 (2015) 89–98.
[27] G. Kitis, G.S. Polymeris, E. Şahiner, N. Meric, V. Pagonis, J. Lumin. 176 (2016) 32–39.
[28] V. Angeli, G. Kitis, G.S. Polymeris, E. Şahiner, N. Meric, Appl. Radiat. Isot. 143 (2019) 156–162.
[29] H. Kroll, P.H. Ribbe, Am. Mineral. 72 (1987) 491–506.
[30] G.S. Polymeris, E. Theodosoglou, G. Kitis, N.C. Tsirliganis, A. Koroneos, K. M. Paraskevopoulos, Medit. Archaeol. and Archaeom. 13 (2013) 155–161.
[31] V. Pagonis, G.S. Polymeris, G. Kitis, Radiat. Meas. 82 (2015) 93–101.
[32] C. Schmidt, J. Friedrich, G. Adamiec, A. Chruscinska, M. Fasolid, S. Kreutzer, M. Martini, L. Panzeri, G.S. Polymeris, K. Przegietka, P.G. Valla, G.E. King, C. David, W. Sanderson, Radiat. Meas. 110 (2018) 14–24.
[33] G. Kitis, N.G. Kiyak, G.S. Polymeris, Nucl. Instrum. Methods Phys. Res. B 359 (2015) 60–63.
[34] I.K. Sfampa, G.S. Polymeris, V. Pagonis, G. Kitis, Radiat. Phys. Chem. 165 (2019) 108386 (2019).
[35] L. Botter-Jensen, S.W.S. McKeever, Wintle, Optically Stimulated Luminecence Dosimetry, Elsevier, Amsterdam, 2003.
[36] G. Kitis, V. Pagonis, Radiat. Meas. 43 (2008) 737–741.
[37] D. Afouxenidis, G.S. Polymeris, N.C. Tsirliganis, G. Kitis, Radiat. Protect. Dosim. 149 (4) (2012) 363–370 (2012).
[38] H.G. Balian, N.W. Eddy, Nucl. Instrum. Methods 145 (1977) 389–395.
[39] E. Şahiner, M.K. Erturaç, G.S. Polymeris, N. Meriç, Radiat. Meas. 120 (2018) 163–169.
[40] V. Pagonis, M. Jain, K.J. Thomsen, A.S. Murray, J. Lumin. 153 (2014) 96–103.
[41] G.S. Polymeris, I.K. Sfampa, M. Niora, L. Malletzidou, E.C. Stefanaki, V. Giannoulatou, V. Pagonis, G. Kitis, J. Lumin. 195 (2018) 216–224.